AIP Applied Physics Letters

Fabrication and luminescent properties of core-shell InGaN/GaN multiple quantum wells on GaN nanopillars

J.-R. Chang, S.-P. Chang, Y.-J. Li, Y.-J. Cheng, K.-P. Sou, J.-K. Huang, H.-C. Kuo, and C.-Y. Chang

Citation: Applied Physics Letters **100**, 261103 (2012); doi: 10.1063/1.4731629
View online: http://dx.doi.org/10.1063/1.4731629
View Table of Contents: http://scitation.aip.org/content/aip/journal/apl/100/26?ver=pdfcov
Published by the AIP Publishing

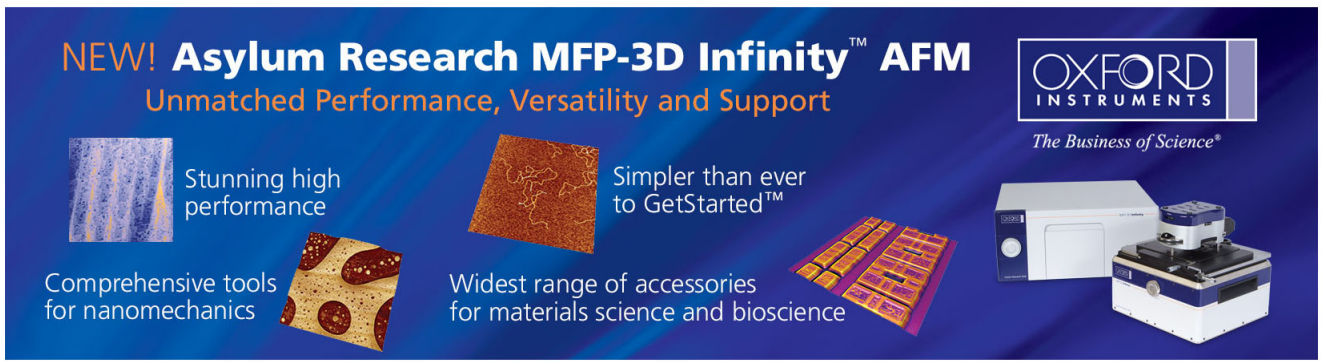

Fabrication and luminescent properties of core-shell InGaN/GaN multiple quantum wells on GaN nanopillars

J.-R. Chang,[1] S.-P. Chang,[1,2] Y.-J. Li,[1] Y.-J. Cheng,[2,3] K.-P. Sou,[2] J.-K. Huang,[2] H.-C. Kuo,[2] and C.-Y. Chang[1]
[1]*Department of Electronics Engineering, National Chiao Tung University, 1001 Ta Hsueh Rd., Hsinchu 300, Taiwan*
[2]*Department of Photonics and Institute of Electro-Optical Engineering, National Chiao Tung University, 1001 Ta Hsueh Rd., Hsinchu 300, Taiwan*
[3]*Research Center for Applied Sciences, Academia Sinica, Taipei 11529, Taiwan*

(Received 30 April 2012; accepted 11 June 2012; published online 25 June 2012)

Core-shell InGaN/GaN multiple quantum wells (MQWs) on GaN nanopillars were fabricated by top-down etching followed by epitaxial regrowth. The regrowth formed hexagonal sidewalls and pyramids on the nanopillars. The cathodoluminescence of MQWs blue shifts as the location moves from top to bottom on both the pillar sidewalls and pyramid facets, covering a spectral linewidth of about 100 nm. The MQWs on the pillar sidewalls have a higher InN fraction than those on the pyramid facets. The photoluminescent wavelength is stable over two orders of carrier density change due to the smaller quantum confined Stark effect on the nanopillar facets. © *2012 American Institute of Physics*. [http://dx.doi.org/10.1063/1.4731629]

In recent years, one dimensional GaN nano structures have gained significant research interests as a potential alternative design to improve the efficiency of the commonly used planar structure GaN light emitting diodes (LEDs). The nanopillar structure provides several advantages over the planar structure. The nanopillar exhibits a significantly reduced defect density because it has only a small area of contact with the growth template. This small footprint reduces strain built up from the lattice and thermal expansion coefficient mismatch between the GaN nanopillar and the growth template,[1–3] thus reducing piezoelectric polarization and improving electron-hole recombination efficiency.[4,5] The reduced strain also allows for higher InN fraction in InGaN/GaN multiple quantum wells (MQWs) for green-red color emission applications.[6–8] These advantages have been demonstrated in MQWs grown in the nanopillar axial direction, which is often the c-axis crystal direction. The nanopillar offers an additional option to grow MQWs on the pillar surfaces in a core-shell geometry. These surfaces can be nonpolar or semipolar crystal planes with zero or low polarization fields. The MQWs grown on these planes have a lower carrier density dependent wavelength change and a higher radiative recombination efficiency.[9–11] This structure can also result in a much larger active surface area than found in MQWs grown on the nanopillar axial direction. Due to the nature of their three dimensional structure, the growth and emission properties of core-shell MQWs can vary with different crystal planes and require investigation.

GaN nanopillars can be fabricated by either a bottom-up or top-down approach. The former grows vertical nanopillars upward from a substrate by molecular beam epitaxy or hydride vapor phase epitaxy.[6–8] The nanopillars are often formed by self assembly. This approach provides less control over the size and location of nanopillars. The latter approach creates nanopillars by etching a flat substrate downward with circular etching masks,[12] providing improved dimension and pattern control. However, the etching process usually produces damaged surfaces that may require repairs. Here, we report a fabrication process using top-down patterned etching followed by an epitaxial regrowth to create crystalline core-shell MQWs on GaN nanopillar arrays. The regrowth repairs the surface damage caused by the top-down patterned etching. Spatially resolved cathodoluminescence (CL) shows that the emission of MQWs has a strong crystal plane and geometry dependence. The emission covers a spectral width of about 100 nm. Such broad bandwidth emission can be useful in white light LED applications. Photoluminescence (PL) shows that the emission wavelength is stable over two orders of pump power change, which is attributed to the reduced quantum confined Stark effect on the nanopillar facets.

Figures 1(a)–1(d) show the schematic of the fabrication process, along with the corresponding scanning electron microscope (SEM) images. SiO_2 nano disks of 250 nm in diameter with center to center spacing of 800 nm were first patterned on a GaN substrate by imprint lithography. The disks were then used as hard masks in inductively coupled plasma reactive ion etching, which etched down the exposed GaN and formed GaN nanopillars about 1.0 μm tall. The disks were subsequently removed by buffer oxide etching, leaving arrays of GaN nanopillars (Figs. 1(a) and 1(c)). The sample was then subject to GaN epitaxial regrowth, followed by MQW growth, as shown in Fig. 1(b). Despite the pillars' original cylindrical shape, the regrowth formed crystalline sidewalls and pyramid facets on the nanopillars, as shown in Fig. 1(d). The GaN regrowth took place at 805 °C. The lower temperature was intentionally chosen to form hexagonal pyramids on the tops of nanopillars and to have higher InN fraction in the InGaN quantum wells. Six pairs of InGaN/GaN MQWs were subsequently grown at 700 and 805 °C, respectively, for wells and barriers. The growth pressure was 300 mbar. The TMIn and TMGa flux were 250 and 76 sccm,

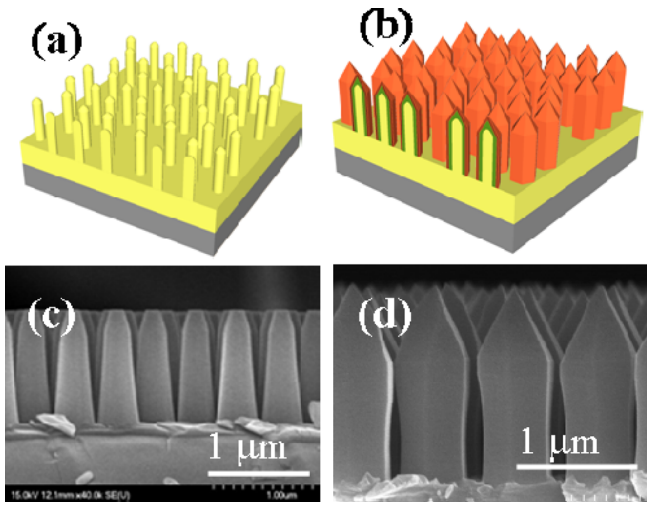

FIG. 1. (a) and (b) Schematic of fabrication steps; (c) and (d) corresponding SEM images.

respectively, and the respective growth times of the wells and barriers were 125 and 300 s.

CL was used to investigate the emission properties of the fabricated nanopillars. A cross section SEM image was first taken (Fig. 2(a)). The detection mode was then switched to cathodoluminescent measurement under the same magnification. The integrated spectrum over the whole imaged area was found to have a broad emission bandwidth of about 100 nm (Fig. 2(b)). The 369 nm peak is from the GaN band edge transition. Figure 2(c) is the 369 nm emission image, which is rather weak because most of the excitation energy is absorbed by MQWs. Figures 2(d)–2(i) present the spectrally resolved images, showing the location dependent emission wavelength change of the core-shell MQWs. The MQW emission wavelength red shifts from 420 to 520 nm as the locations are scanned from the bottom to the upper portion of the nanopillars. The same CL analysis was also performed from a top view (Figs. 3(a)–3(f)). The emission of MQWs located at the bottom portion of the pyramid facets is around 450 nm. The emission red shifts to 530 nm with decreasing intensity as the location move toward the apex. It is worth noting that the 450 nm emission from the bottom of the pyramid facets (Fig. 3(b)) is different from the 520 nm emission from the adjacent upper pillar sidewalls (Fig. 2(i)), implying a large InN fraction difference between the InGaN/GaN MQWs grown on the sidewalls and the pyramid facets.

Figure 4(a) presents the SEM top view of the nanopillars, showing two types of pyramid structures. One, labeled H, is a regular hexagonal pyramid. The other, labeled T, has the same hexagonal pyramid facets in the bottom portion but three alternate facets, labeled 1, 3, and 5 in Fig. 4(b), take over to form triangular pyramid facets in the upper portion. Figure 4(c) presents a schematic illustration for this facet evolution. The red dashed lines depict a regular hexagonal pyramid, while the blue dashed lines depict a triangular pyramid. The facet 2 is over taken by the merger of two adjacent facets 1 and 3 in the upper portion, resulting in a hexagonal to triangular pyramid evolution. The cause of this transformation is still not understood and requires further investigation.

Figure 5(a) presents a cross section transmission electron microscopy (TEM) image of this pillar taken through the pyramid center along the dashed line shown in Fig. 4(b). This cross section was chosen to show both the normal facet growth and the peculiar pyramid facet evolution mentioned above. From the electron diffraction pattern, the inclined pyramid facets and the pillar sidewalls are, respectively, identified as {10-11} and {10-10} planes, revealing the core-shell MQW structure. Figure 5(a) also shows the QW and barrier thickness, and InN fractions at various locations. The InN fraction was measured by the energy dispersive x-ray spectroscopy. The six InGaN MQWs, showing a dark color in contrast to the GaN barriers, provide snap shots of the

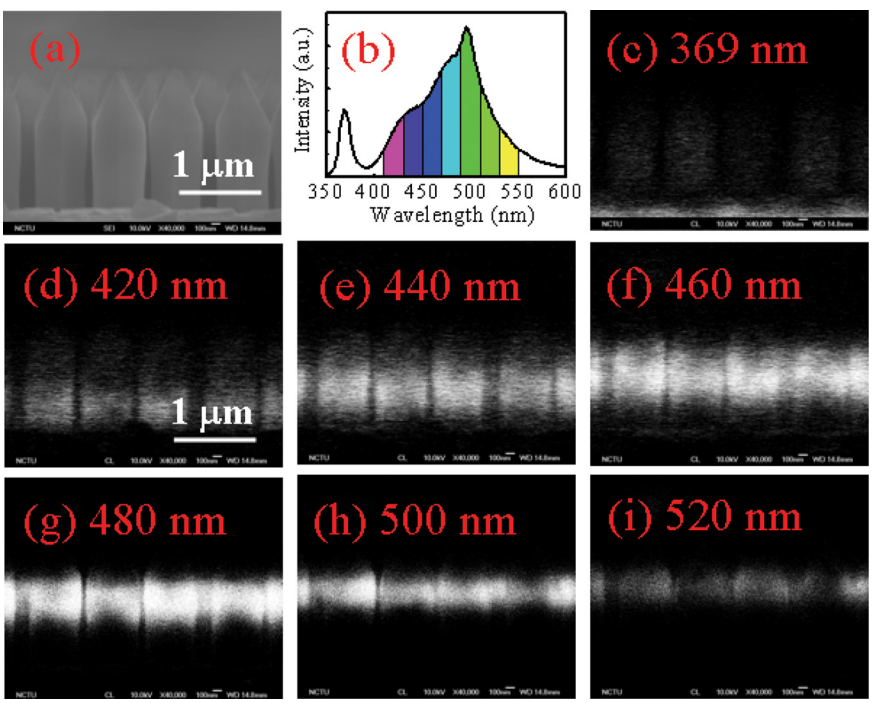

FIG. 2. (a) SEM cross section view of the fabricated nanopillars. (b) The CL spectrum integrated over the imaged area shown in (a). (c)–(i) The spectrally resolved CL images showing location dependent emission wavelength.

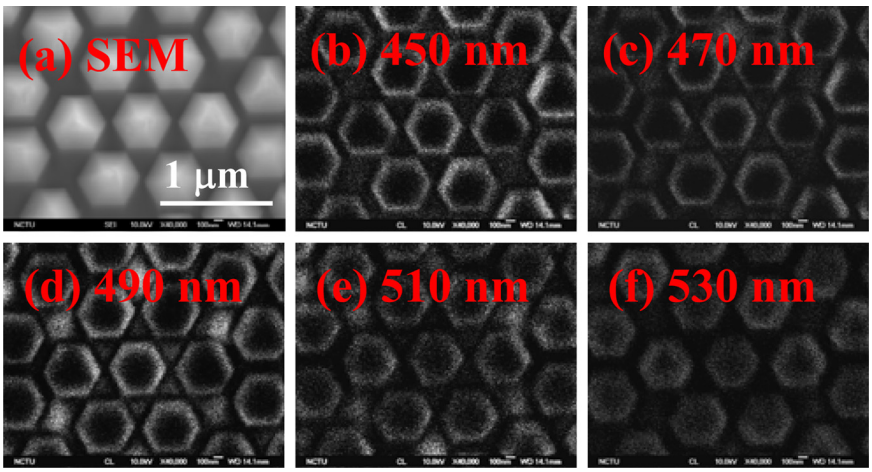

FIG. 3. (a) SEM top view of nanopillars showing the hexagonal pyramids. (b)–(f) Spectrally resolved CL images showing location dependent emission wavelength.

evolution. The first InGaN QW shows a pyramid contour on the top and slightly tapered pillar sidewalls. This indicates that the GaN regrowth has grown a pyramid on the top while the pillar still has a slightly tapered shape prior to the first QW growth. The first QW pyramid contour is rather symmetric. As the growth continues, the symmetry is broken. The QWs on the upper right portion gradually protrude because of the facet evolution among facets 1, 2, and 3, as shown in Fig. 4(c). A sharp turning corner is developed at the junction between the pyramid facets and pillar sidewalls as GaN grows from the first to second QW (dotted line circles in Fig. 5(b)), indicating the formation of crystalline facets. The growth rate of the upper part of pillar sidewall is faster than that of the lower part, producing a pillar that gradually narrows towards the base. The slower growth rate at the bottom is due to the limited available source diffused to the bottom. The 25% InN fraction at the upper sidewall is much greater than the 16% at the adjacent pyramid facet, indicating that the {10-10} plane can accommodate higher InN fraction in InGaN MQWs than the {10-11} plane. The percentage drops to 11.6% in the bottom portion of nanopillars, due to the less available In source diffused to the bottom. This large facet and geometry dependent InN fraction change produce a broad 100 nm overall emission bandwidth, which could be useful in white light LED applications.

The PL property of the sample was investigated by pumping the sample using a 325 nm HeCd laser, with the measured PL spectrum versus pump power shown in Fig. 6. The PL spectrum has a broad linewidth of about 100 nm, in consistent with the CL result. The spectral position however remains fairly stable over the two orders of pump power change. In conventional planar MQW design, where MQWs are grown in the c-plane direction, the emission often blue shifts as carrier density increases. This is due to the quantum confined Stark effect caused by the strong polarization field in the c-plane direction. The core-shell MQWs are on the {10-10} nonpolar and {10-11} semipolar nanopillar facets, which have respectively zero and fairly small polarization fields. As a result, the quantum confined Stark effect is greatly reduced and the emission wavelength can remain stable over two orders of carrier density change.

In summary, we have fabricated core-shell MQW nanopillar arrays by patterned top-down etching and a subsequent epitaxial regrowth. The regrowth results in crystalline

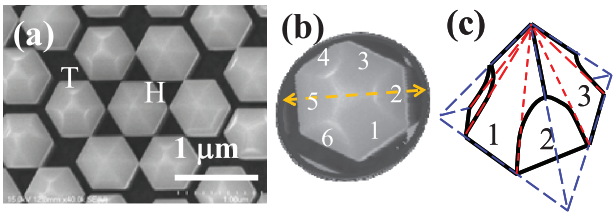

FIG. 4. (a) SEM top view of nanopillars showing two different pyramid geometries (labeled as H and T). (b) Close view of the pyramid T. (c) Schematic showing the facet evolution of pyramid T, transforming from hexagonal to triangular pyramid facets from bottom to top.

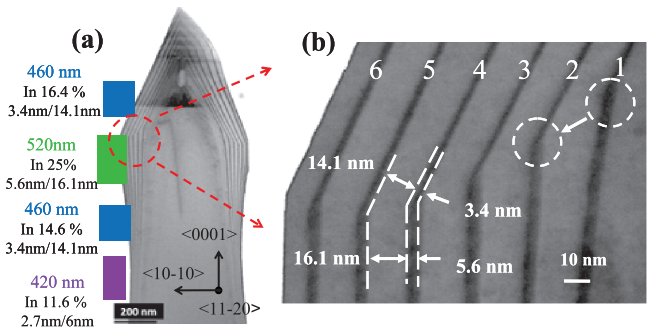

FIG. 5. (a) TEM cross section view of a nanopillar, showing the growth of six QWs (dark colored lines), the InN fraction, and well/barrier thickness. (b) Close view at the pyramid facet and pillar sidewall junction.

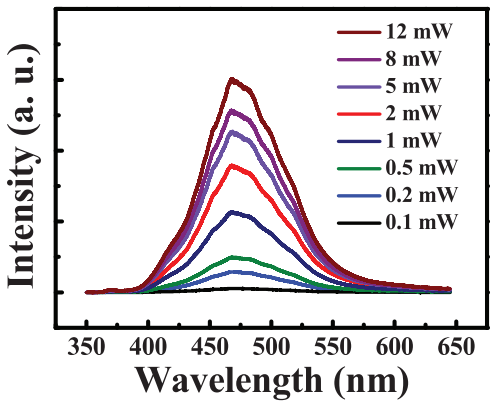

FIG. 6. PL spectrum versus pump power. Negligible wavelength shift over two orders of pump power change.

hexagonal pyramid nanopillars with {10-10} nonpolar sidewalls and {10-11} semipolar pyramid facets. The MQWs grown on these facets have large location dependent InN fraction variations. The emission has a broad spectrum covering from 420 to 520 nm. The PL spectrum remains fairly stable over two orders of carrier density change due to the low polarization field of nonpolar and semipolar facets. The broad emission linewidth and low polarization field make the core-shell MQW pillar structure an attractive design for LED lighting applications.

The authors would like to thank Dr. T. C. Hsu and M. H. Shieh of Epistar Corporation for their technical supporting. This work was financially supported by the National Science Council of Taiwan under contract NSC 100-2112-M-001-021-MY3.

[1]H. J. Chang, Y. P. Hsieh, T. T. Chen, Y. F. Chen, and C. T. Liang, Opt. Express **15**, 9357 (2007).
[2]J. Renard, R. Songmuang, G. Tourbot, C. Bougerol, B. Daudin, and B. Gayral, Phys. Rev. B **80**, 121305 (2009).
[3]Q. Li and G. T. Wanga, Appl. Phys. Lett. **97**, 181107 (2010).
[4]Y.-L. Chang, J. L. Wang, F. Li, and Z. Mia, Appl. Phys. Lett. **96**, 013106 (2010).
[5]Y. J. Hong, C.-H. Lee, A. Yoon, M. Kim, H.-K. Seong, H. J. Chung, C. Sone, Y. J. Park, and G.-C. Yi, Adv. Mater. **23**, 3284 (2011).
[6]H. Sekiguchi, K. Kishino, and A. Kikuchi, Appl. Phys. Lett. **96**, 231104 (2010).
[7]H. P. T. Nguyen, K. Cui, S. Zhang, M. Djavid, A. Korinek, G. A. Botton, and Z. Mi, Nano Lett. **12**, 1317 (2012).
[8]H.-W. Lin, Y.-J. Lu, H.-Y. Chen, H.-M. Lee, and S. Gwo, Appl. Phys. Lett. **97**, 073101 (2010).
[9]R. Koester, J.-S. Hwang, D. Salomon, X. Chen, C. Bougerol, J.-P. Barnes, D. L. S. Dang, L. Rigutti, A. de Luna Bugallo, G. Jacopin, M. Tchernycheva, C. Durand, and J. Eymery, Nano Lett. **11**, 4839 (2011).
[10]C.-H. Lee, J. Yoo, Y. J. Hong, J. Cho, Y.-J. Kim, S.-R. Jeon, J. H. Baek, and G.-C. Yi, Appl. Phys. Lett. **94**, 213101 (2009).
[11]T.-W. Yeh, Y.-T. Lin, B. Ahn, L. S. Stewart, P. D. Dapkus, and S. R. Nutt, Appl. Phys. Lett. **100**, 033119 (2012).
[12]Q. Li, K. R. Westlake, M. H. Crawford, S. R. Lee, D. D. Koleske, J. J. Figiel, K. C. Cross, S. Fathololoumi, Z. Mi, and G. T. Wang, Opt. Express **19**, 25528 (2011).